Electronic Supporting Information

Achieving ultra-trace analysis and multi-light driven photodegradation toward phenolic derivatives via a bifunctional catalyst derived from Cu(I)-complex-modified polyoxometalate

Shuang Li, Bingqian Wang, Guocheng Liu,* Xiaohui Li, Chang Sun, Zhong Zhang,* and Xiuli Wang*

College of Chemistry and Materials Engineering, Professional Technology Innovation Center of Liaoning Province for Conversion Materials of Solar Cell, Bohai University, Jinzhou 121013, China.

X-ray crystallography

A suitable crystal was collected on a Bruker SMART APEXII system (λ = 0.71073 A) equipped with Mo Kα radiation (λ = 0.71073 Å) at 293(2) K. The structure of **1** was solved by direct methods and refined by a full-matrix least-squares fitting on F^2 using the Olex2 program [1]. CCDC 2263177 for **1** contains the supplementary crystallographic data for this paper.

Materials and instruments

The ligand [N,N'-bis(3-methylpyridin-yl)naphthalene-2,6-dicarboxamide (L)] was synthesized through the methods reported previously [2]. Other chemicals were commercially purchased and used without further purification. The elemental analyses (carbon, hydrogen, and nitrogen) of **1** were performed on a PerkinElmer 2400C elemental analyzer. The FT-IR spectra were tested by a Varian 640 FT-IR spectrometer from 500−4000 cm^{-1}. PXRD information was collected by the D/teX Ultra diffractometer with Cu Kα (λ=1.5406 Å) radiation in the range of 5–50°. X-ray photoelectron spectroscopy (XPS) was measured on a Thermo Scientific K-Alpha spectrometer with an Al Kα X-ray source. The UV-Vis diffuse reflection spectrum was obtained on a spectrophotometer (Lambda, Model 750). The UV-Vis absorption spectrum was obtained on an SP-1900 UV-Vis spectrophotometer. The Mott-Schottky studies, the electrochemical impedance spectroscopy and the photocurrent response experiment were used by CHI 760 workstation combining with a 300 W Xe lamp (PLS-SXE300/300UV). The photochemical reactions were carried by a set of photocatalytic reaction device (CEL-LAB500, Zhongjiao Jinyuan) with a cryogenic bath (DC-0506) for controlling the reaction temperature at 25 °C. The fluorescence spectra were tested on a Hitachi F-4500 fluorescence spectrometer. Raman spectra were performed on a Renishaw Raman (LabRAM HR Evolution) microscope.

Preparation of working electrode for EIS and Mott-Schottky experiment

0.5 × 2 cm^2 carbon cloth (CC) was cut out and treated with HNO_3, H_2O, and ethanol in sequence. Then vacuum dry was performed at 80 °C for 10 h. The electrode material based on complex **1** was prepared as following: activated carbon (2 mg), complex **1** (2 mg) and Poly (vinylidene fluoride) (PVDF) (1 mg) were ground together in an agate mortar for 1 h to obtain a mixture; 0.10 mL N-methy pyrrolidone (NMP) was added and stirred to get a black paste; The paste was coated onto one side of the treated CC. Finally, the working electrode was vacuum-

dried at 80 °C for 12 h.

Photocurrent response measurement

The photocurrent response was tested in 0.2 M Na_2SO_4 solution and by using xenon lamp as the light source with a classic three-electrode system on a CHI760 electrochemical workstation. In the three-electrode system, the reference electrode is Ag/AgCl electrode, the counter electrode is Pt plate, and the working electrode is fluorine-doped tin oxide (FTO) glass covered with crystal sample of **1**. Preparation of the working electrode for photocurrent response measurement is as follows: 2 mg of complex **1** was dispersed into 400 μL methanol. The ultrasonic treatment was performed subsequently until **1** was completely dispersed. Then the suspension of **1** was evenly dripped onto the conductive surface of the FTO glass and naturally dried. Finally, the remaining part of the FTO glass was isolated with epoxy resin adhesive. After all the preparation, xenon lamp was used to illuminate the working electrode and cut manually every 20 seconds. The whole experiment was proceeding in a continuous and repeated on/off cycle.

Tests of peroxidase-like activity

The catalytic reaction of 4-AAP and phenol was used to explore the enzymatic activity of peroxides. In the typical experiment, 4-AAP (2 $mg \cdot mL^{-1}$), **1** (0.5 $mg \cdot mL^{-1}$), phenol (6 mM) and H_2O_2 (5 mM) were added to a 5 mL centrifuge tube and set the total volume of the solution to 3 mL. At room temperature, the reaction was carried out 30 min. Then the absorbance of the reaction solution at 501 nm was record using an UV-Vis spectrometer.

Photoluminescent experiments for the mechanism of 1 as peroxidase

Terephthalic acid (TA) was selected as a fluorescent probe to simulate the ·OH produced by peroxidase for further analysis. First, four experimental groups: (I) TA; (II) TA and **1**; (III) TA and H_2O_2; (IV) TA, H_2O_2 and **1** in a 5 mL centrifuge tube and set the total volume to 3 mL, react in the dark for 12 h and centrifuge. Then, the fluorescence spectrum of the mixed solution was detected at an excitation wavelength of 326 nm.

Photocatalytic degradation of phenolic compounds

Phenol was selected as a representative and sunlight was used as the irradiation to investigate the catalytic activity of complex **1** with the optimal conditions. All the reactions were carried out on bright sunny days from 12 a.m. to 2 pm in summer and autumn at Jinzhou, China. Typically, the photocatalytic degradation experimental methods are described as follows. 5.0 mg of complex **1** was dispersed in 10 mL solution with 400 $mg \cdot L^{-1}$ phenolic compounds (pH = 8) and reached the adsorption and desorption equilibrium after stirring for 30 min in the dark. Then a certain amount of fresh 30% H_2O_2 (200 μL) was added to the mixture. After that, the suspension was irradiated under the sun light irradiation.

After that, 0.20 mL of the degraded solution was diluted to 1.80 mL with PBS (pH 1–12), and then mixed with 0.30 mL of 16.68 $mmol \cdot L^{-1}$ $K_3Fe(CN)_6$ in 0.25 mol L^{-1} $NaHCO_3$, as well as 0.30 mL of 4.16 $mmol \cdot L^{-1}$ 4-AAP in 0.25 $mol \cdot L^{-1}$ $NaHCO_3$. The mixed solution was reacted for 5 min at room temperature. The absorbance (about 505 nm) was monitored by UV-vis

spectrophotometer.

The calculation method of detection limit

The following formula was used to calculate the limit of detection (LOD) of **1** to phenolic compounds:

$$LOD = \frac{S/N \cdot \sigma}{K}$$

S/N is the signal-to-noise ratio, and usually the value is 3. σ is the standard deviation, and K is the linear regression slope [3,4].

Scheme S**1** Structural diagram of the ligand (L) in this work.

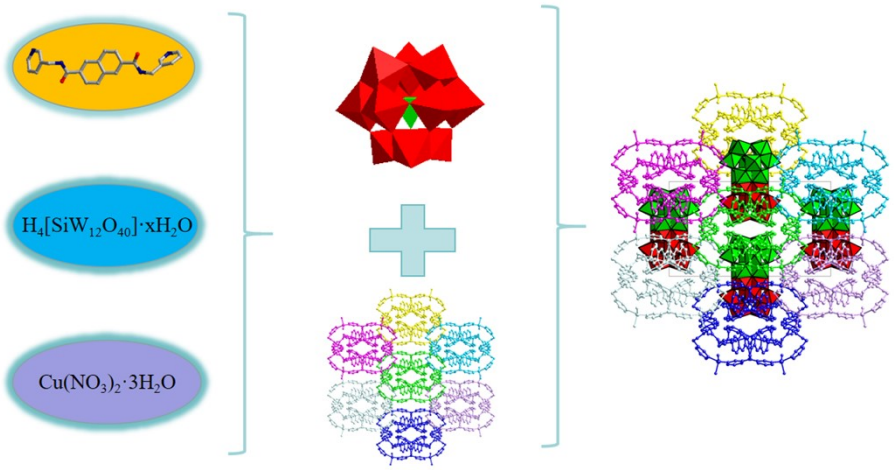

Scheme S2 The schematic view of the synthesis of complex **1**.

Table S1. Crystallographic data of complex **1**.

Complex	**1**
Empirical formula	$C_{96}H_{88}Cu_4N_{16}O_{52}SiW_{12}$
Formula weight	4786.27
Crystal system	monoclinic
Space group	*C2/c*
a/Å	34.8398(11)
b/Å	15.9468(14)
c/Å	27.5958(19)
α/°	90.00
β/°	128.799(2)
γ/°	90.00
V/Å^3	11948.8(7)
Z	4
D_c (g cm^{-3})	2.661
μ/(m m^{-1})	12.299
F(000)	8840.0
Reflection collected	178587
Data/restraints/parameters	10534/13/819
Goodness on F^2	1.088
Final R indexes [I>=2σ (I)]	R_1 = 0.0360, wR_2 = 0.0926
Final R indexes [all data]	R_1 = 0.0537, wR_2 = 0.1054
CCDC	2263177

Table S2. Selected bond distances (Å) of complex **1**.

Complex **1**			
W1−O4$^{\#1}$	2.366(6)	W5−O5	1.697(6)
W1−O10	1.922(6)	W5−O9	1.901(6)
W1−O14	1.924(6)	W5−O10	1.891(7)
W1−O15	1.705(7)	W5−O12	1.913(6)
W1−O23	1.898(6)	W5−O22	2.342(6)
W1−O26	1.906(6)	W5−O24	1.936(6)
W2−O11	1.705(6)	W6−O9	1.933(6)
W2−O12$^{\#1}$	1.884(6)	W6−O13	1.926(6)
W2−O13	1.933(7)	W6−O17	1.899(6)
W2−O22	2,349(6)	W6−O19$^{\#1}$	1.909(6)
W2−O24	1.909(6)	W6−O22	2.357(6)
W2−O26$^{\#1}$	1.908(7)	W6−O25	1.684(7)
W3−O4$^{\#1}$	2.348(6)	Cu1−O1W	2.064(16)
W3−O3	1.700(7)	Cu1−O2W	1.198(14)
W3−O14	1.912(7)	Cu1−N1	2.028(10)
W3−O17	1.905(6)	Cu1−N2$^{\#3}$	2.141(10)
W3−O18	1.922(6)	Cu2−N4	1.896(11)
W3−O21	1.930(6)	Cu2−N3	1.896(10)
W4−O4$^{\#1}$	2.336(6)	Cu2−O1$^{\#4}$	2.478(10)
W4−O16	1.708(6)	Si−O4	1.625(6)
W4−O18$^{\#1}$	1.898(6)	Si−O4$^{\#1}$	1.625(6)
W4−O19	1.897(6)	Si−O22	1.621(6)
W4−O21	1.935(6)	Si−O22$^{\#1}$	1.621(6)
W4−O23	1.947(6)		

$^{\#1}$ $1-x, y, 1/2-z$; $^{\#2}$ $-1/2+x, 1/2+y, z$; $^{\#3}$ $1-x, 1-y, 1-z$; $^{\#4}$ $1-x, y, 3/2-z$

Table S3. Bond valence sum (BVS) calculations of Si, W and Cu atoms in **1**.

Complex **1**			
Si1	4.18	W3	6.11
Cu1	0.97	W4	6.07
Cu2	0.72	W5	6.21
W1	6.12	W6	6.19
W2	6.18		

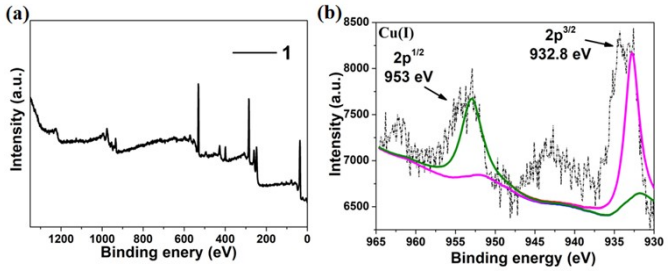

Fig. S1 The XPS spectra patterns of (a) **1**, (b) Cu(I) in **1**.

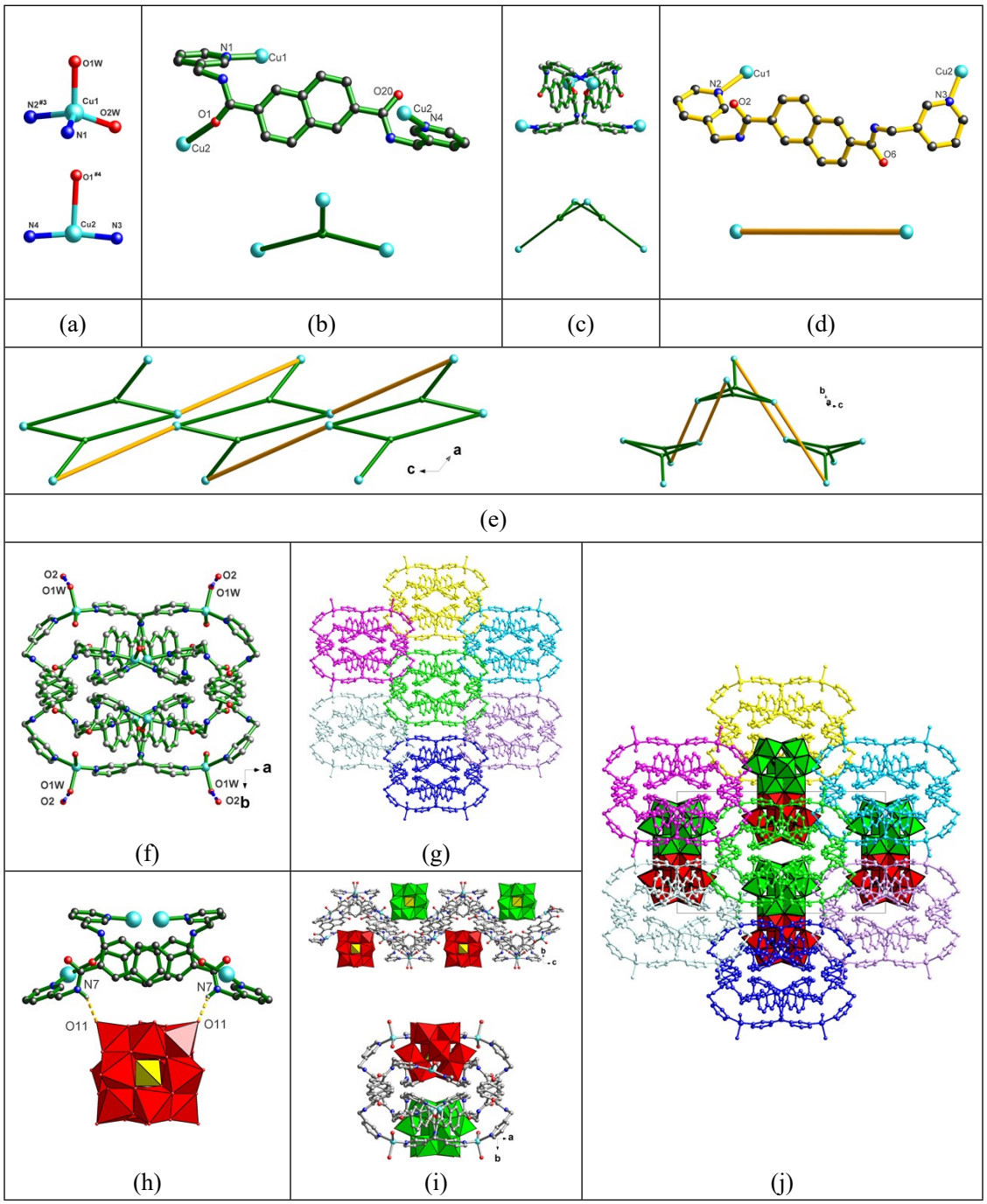

Chart S1. The structural units of complex **1**. (a) The coordinated modes of Cu1 and Cu2. (b) μ_3-L. (c) Cu_4 subunit extended by μ_3-L. (d) μ_2-L. (e) Schematic view of 1D Cu-L nanoribon based on

Cu_4 subunits and pairs of μ_2-L viewed along *b* and *a* axes. (f) H-bonds between different Cu-L nanoribons. (g) 3D supramolecular framework based on Cu-L nanoribons extended by H-bonds [between amide O (O2) and coordinated water (O1W)]. (h) H-bonds between Cu-L nanoribon and SiW_{12} [between amide N (N7) and polyoxometalate (O11)]. (i) 1D wave-like nanoribon based on Cu-L nanoribon and SiW_{12} anions viewed along *a* and *c* axes. (j). 3D stacking structure based on SiW_{12} anions and metal-organic nanoribons.

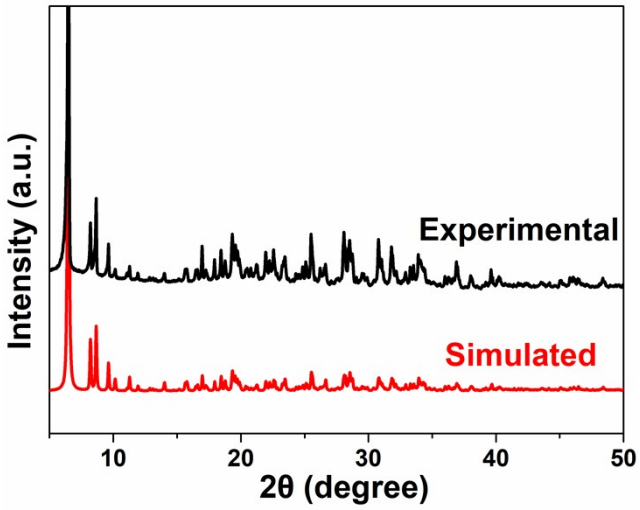

Fig. S2 Comparison of the experimental and simulated PXRD patterns of **1**.

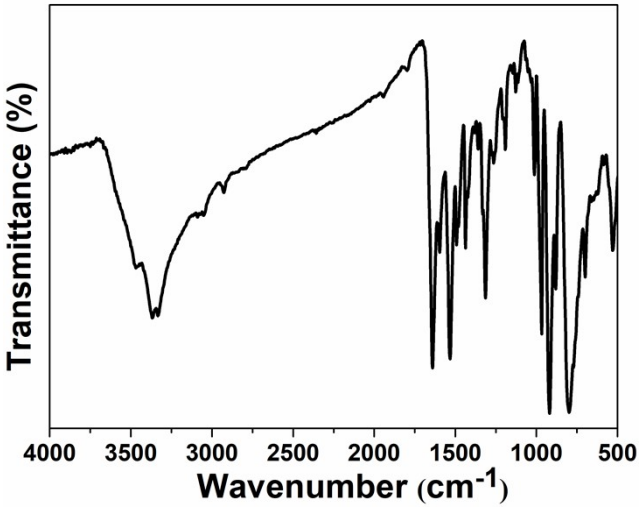

Fig. S3 IR spectrum of **1**.

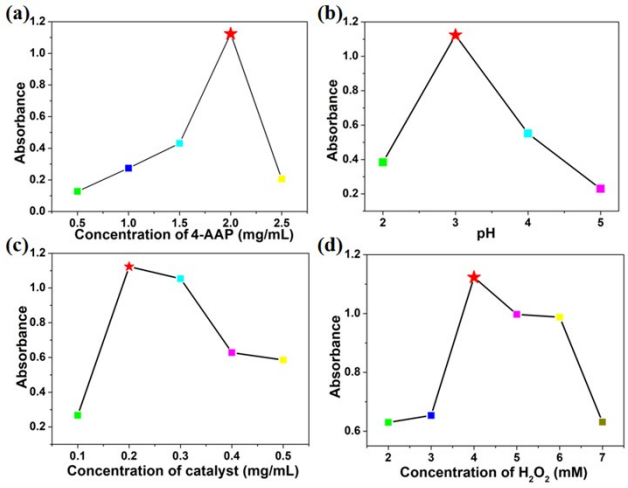

Fig. S4 Effect of (a) concentration of 4-AAP, (b) pH, (c) concentration of catalyst, (d) concentration of H_2O_2 on the colorimetric quantification of phenol.

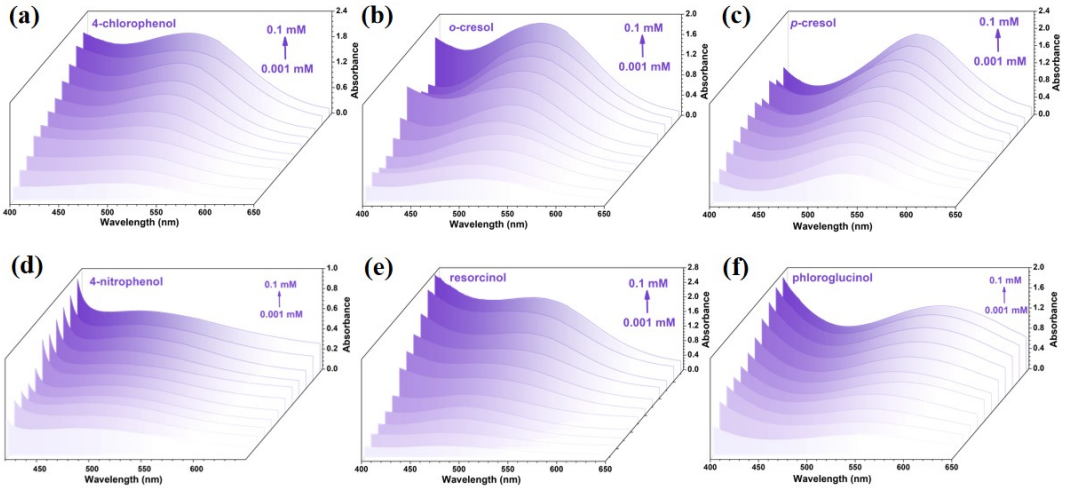

Fig. S5 (a–f) UV-vis absorbance spectra of the colorimetric detection of 4-chlorophenol, *o*-cresol, *p*-cresol, resorcinol and phloroglucinol in the **1**+H_2O_2+4-AAP systems.

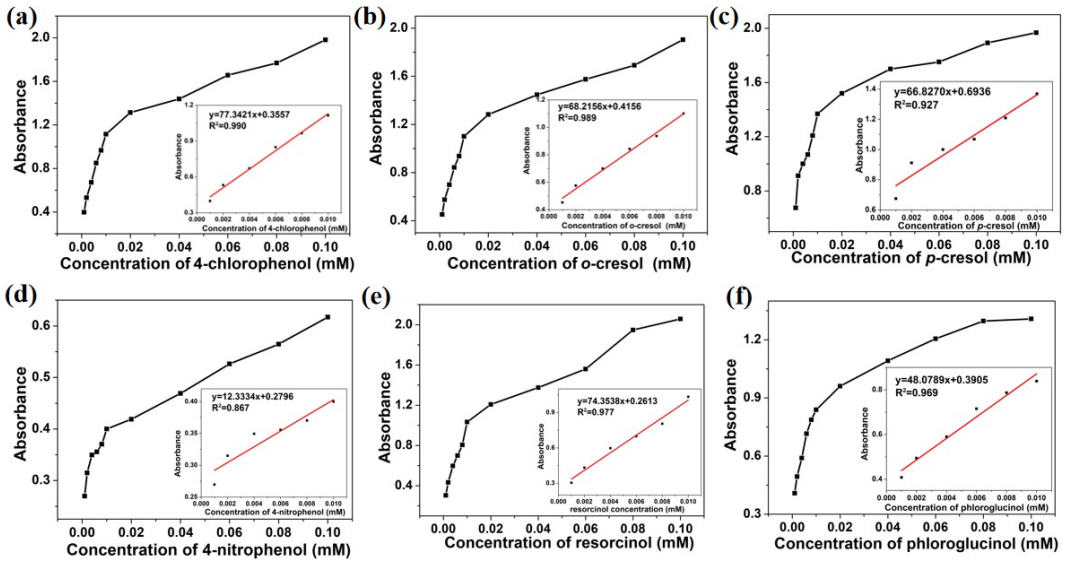

Fig. S6 (a–f) The linear calibration curves of 4-chlorophenol, *o*-cresol, *p*-cresol, 4-nitrophenol,

resorcinol and phloroglucinol detection.

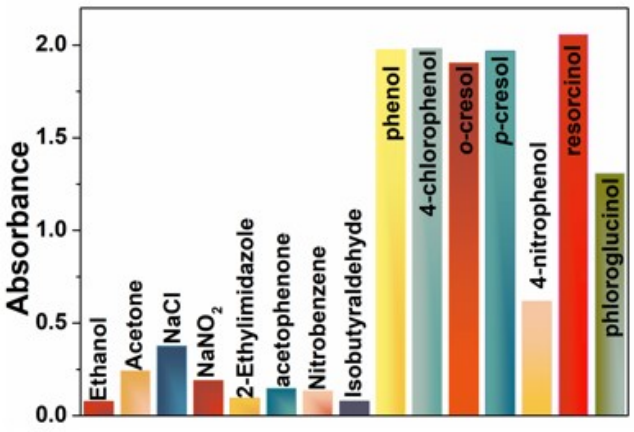

Fig. S7 Selectivity experiment of phenol detection.

Table S4. Comparative table for the detection of phenol using different enzyme mimics.

Catalysts	linear range (μM)	LOD (μM)	References
Fe_3O_4 NPs	1.67–1200	3.79	5
Fe_3O_4/rGO/MOF	10–80	3.33	6
HRP@H-ZIF-8-GOx	0–100	0.86	7
Co-MOF-74	0.5–300	1.02	8
CAT-Fe_3O_4@ZIF-8	5–100	0.7	9
Au@Ni/rGO	1–300	1.6	10
Co-POM	10–1000	1.32	11
1	1–100	0.056	this work

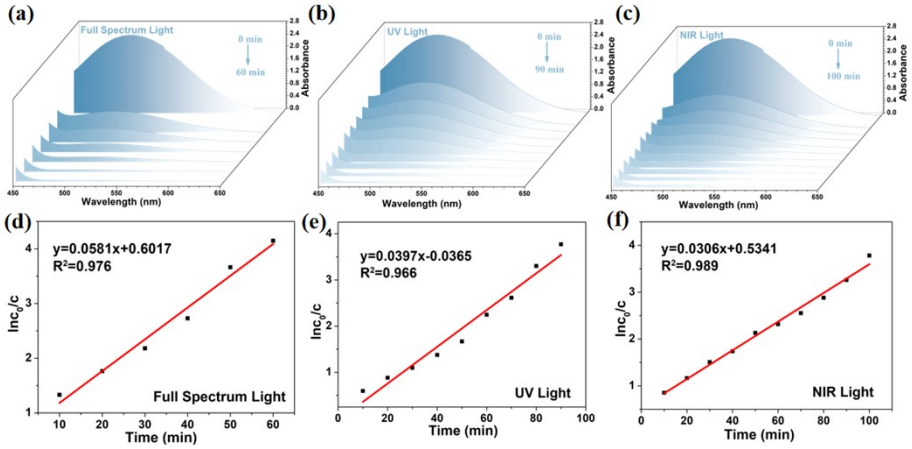

Fig. S8 The photocatalytic degradation of phenol with **1** under different light regimes.

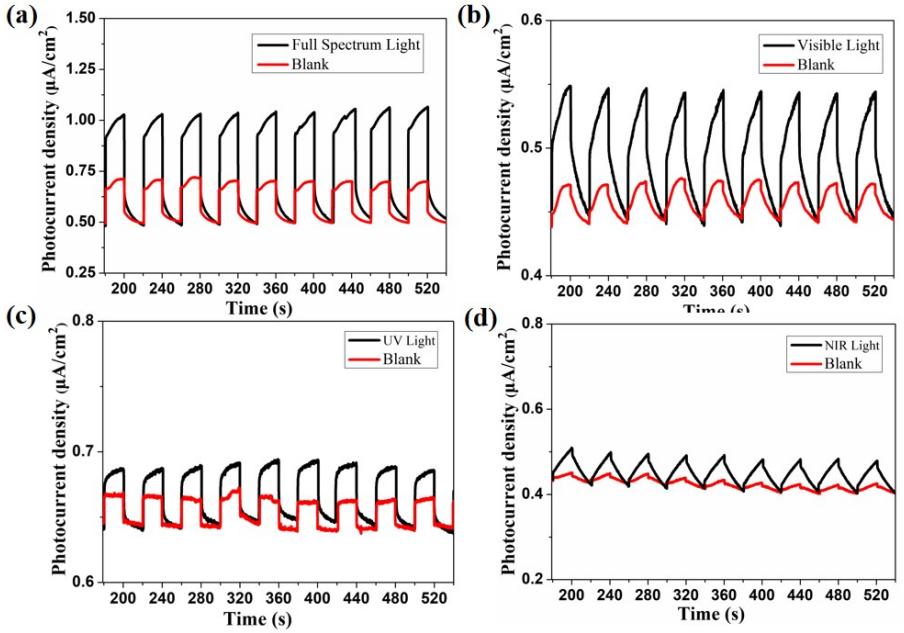

Fig. S9 Transient photocurrent response of **1** and blank under (a) full spectrum light, (b) visible light, (c) UV light, (d) NIR light and corresponding blank.

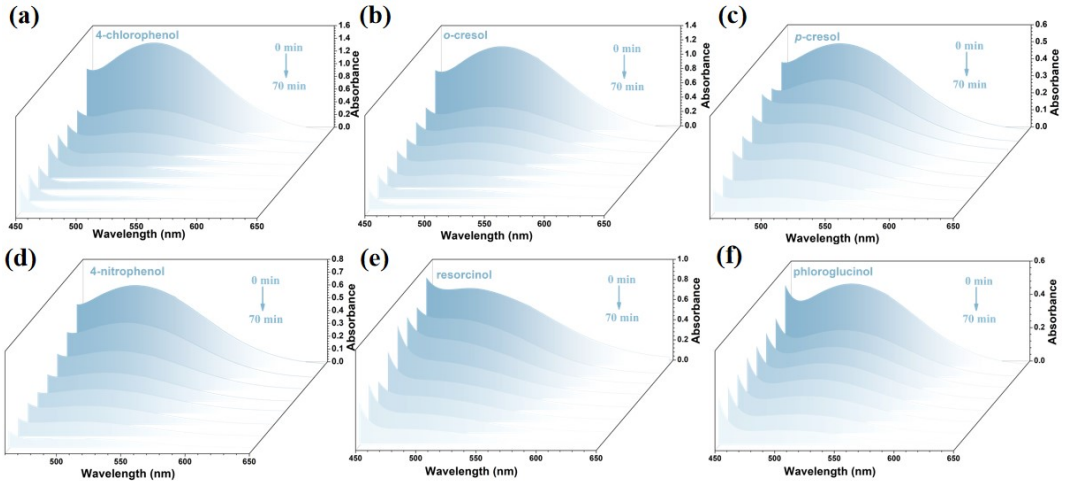

Fig. S10 The photocatalytic degradation of phenolic compounds with **1** under different irradiation times using visible light irradiation.

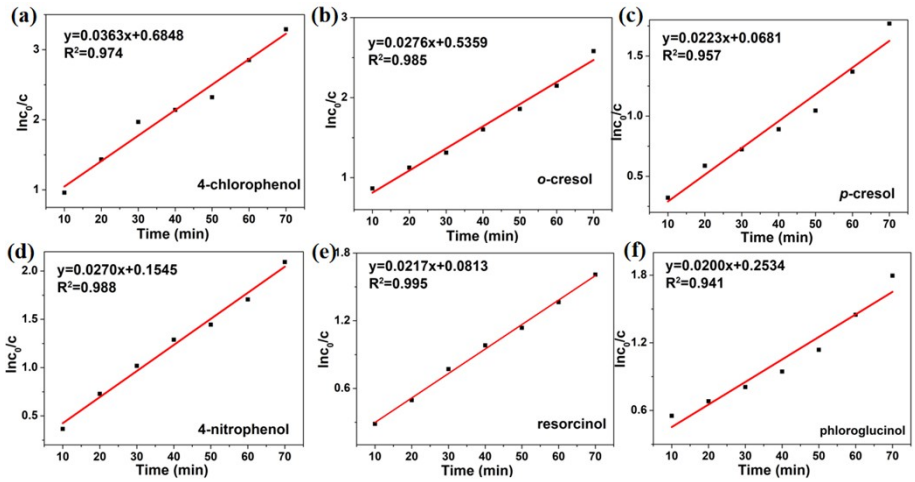

Fig. S11 The linear relationship between $\ln(c_0/c)$ and reaction time (t) of phenolic compounds.

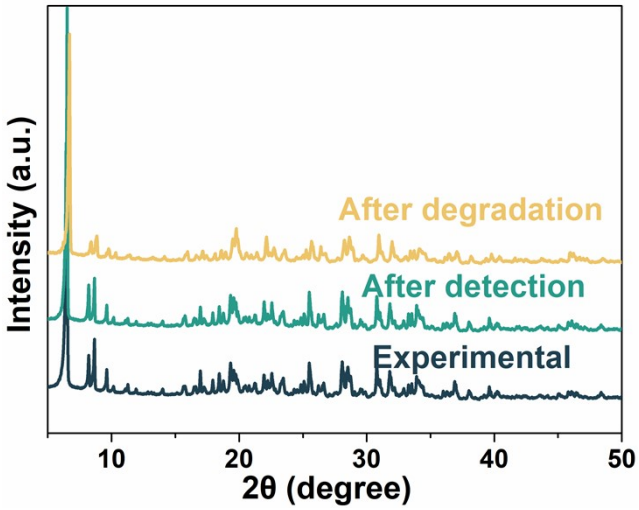

Fig. S12 The PXRD patterns of **1** before and after detection/degradation.

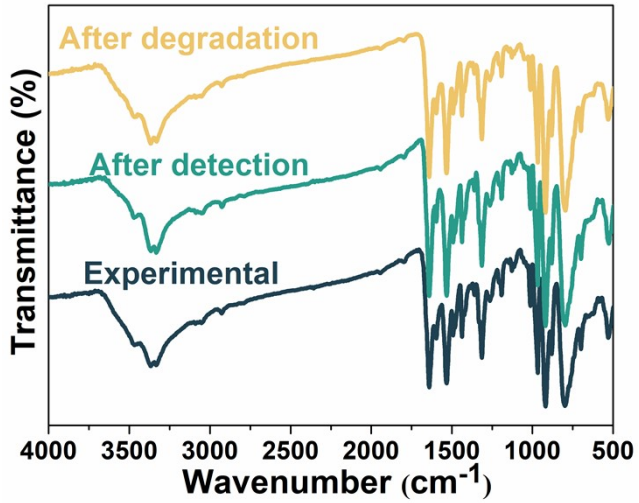

Fig. S13 The IR spectra of **1** before and after detection/degradation.

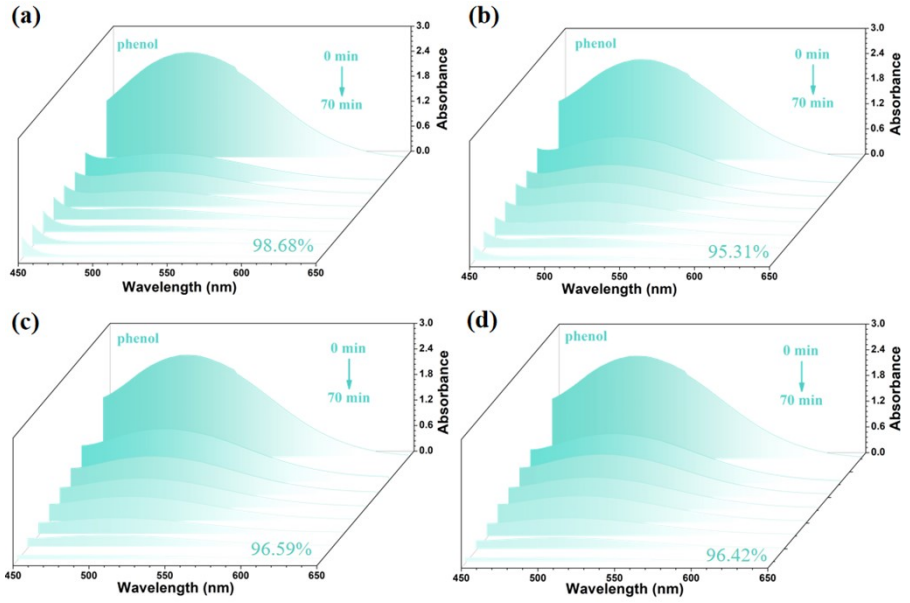

Fig. S14 The photocatalytic degradation of phenol with **1** under sunlight (The experimental dates were September 14, October 11, October 13 and October 15, 2023).

References

[1] G. M. Sheldrick, SHELXTL-97,SHELXS-97, Program for the Solution of Crystal Structures, *University of Göttingen, Germany*, 1997.

[2] M. Sarkar, K. Biradha, Amide-to-Amide Hydrogen Bonds in the Presence of a Pyridine Functionality: Crystal Structures of Bis(pyridinecarboxamido)alkanes, *Cryst. Growth. DES.*, 2006, **6**, 202−208.

[3] H. Han, C. Liu, J. Q. Sha, Y. Wang, C. Y. Dong, M. J. Li, T. Y. Jiao, Ferrocene-reduced graphene oxide-polyoxometalates based ternary nanocomposites as electrochemical detection for acetaminophen, *Talanta*, 2021, **235**, 122751.

[4] S. M. Taghdisi, N. M. Danesh, P. Lavaee, M. Ramezani, K. Abnous, An electrochemical aptasensor based on gold nanoparticles, thionine and hairpin structure of complementary strand of aptamer for ultrasensitive detection of lead, *Sensor. Actuat. B.*, 2016, **234**, 462–469.

[5] S. W. Wu, D. Z. Guo, X. C. Xu, J. M. Pan, X. H. Niu, Colorimetric quantification and discrimination of phenolic pollutants based on peroxidase-like Fe_3O_4 nanoparticles, *Sensor. Actuat. B-Chem.*, 2020, **303**, 127225.

[6] Y. Wang, M. Zhao, C. Hou, X. Yang, Z. Li, Q. Meng, C. Liang, *J. Taiwan. Inst. Chem. E.*, 2019, **102**, 312–320.

[7] H. J. Liu, Y. J. Du, J. Gao, L. Y. Zhou, Y. He, L. Ma, G. H. Liu, Z. Z. Huang, Y. J. Jiang, Compartmentalization of Biocatalysts by Immobilizing Bienzyme in Hollow ZIF-8 for Colorimetric Detection of Glucose and Phenol, *Ind. Eng. Chem. Res.*, 2020, **59**, 42–51.

[8] C. Hou, L. H. Fu, Y. Wang, W. Q. Chen, F. Chen, S. F. Zhang, J. Z. Wang, Co-MOF-74 based Co_3O_4/cellulose derivative membrane as dual-functional catalyst for colorimetric detection and degradation of phenol. *Carbohyd. Polym.*, 2021, **273**, 118548.

[9] J. N. Wang, M. Q. Zeng, Y. H. Zhao, X. M. Zuo, F. R. Meng, H. Y. Jie, F. Lv, Y. Lu, J. B.

Hou, Synergetic integration of catalase and Fe3O4 magnetic nanoparticles with metal organic framework for colorimetric detection of phenol, *Environ. Res.*, 2022, **206**, 112580.
[10] G. Darabdhara, M. R. Das, Dual responsive magnetic Au@Ni nanostructures loaded reduced graphene oxide sheets for colorimetric detection and photocatalytic degradation of toxic phenolic compounds. *J. Haz. Mat.*, 2019, **368**, 365–377.
[11] J. J. Xin, H. J. Pang, Z. X. Jin, Q. Wu, X. J. Yu, H. Y. Ma, X. M. Wang, L. C. Tan, G. X. Yang, Two polyoxometalate-encapsulated two-fold interpenetrating dia metal-organic frameworks for the detection, discrimination, and degradation of phenolic pollutants. *Inorg. Chem.*, 2022, **61**, 16055–16063.